Wang, Di; Schraik, Daniel; Hovi, Aarne; Rautiainen, Miina

Direct estimation of photon recollision probability using terrestrial laser scanning

Published in:
Remote Sensing of Environment

DOI:
10.1016/j.rse.2020.111932

Published: 15/09/2020

Document Version
Publisher's PDF, also known as Version of record

Remote Sensing of Environment 247 (2020) 111932

Contents lists available at ScienceDirect

Remote Sensing of Environment

journal homepage: www.elsevier.com/locate/rse

Direct estimation of photon recollision probability using terrestrial laser scanning

Di Wang[a,*], Daniel Schraik[a], Aarne Hovi[a], Miina Rautiainen[a,b]

[a] Department of Built Environment, School of Engineering, Aalto University, Finland
[b] Department of Electronics and Nanoengineering, School of Electrical Engineering, Aalto University, Finland

ARTICLE INFO

Keywords:
Terrestrial LiDAR
Photon recollision probability
Spectral invariants
Sphere covering
3D model

ABSTRACT

Photon recollision probability p is a spectrally invariant structural parameter and a powerful tool to link canopy optical properties at any wavelengths to model reflectance, transmittance, or absorption of vegetation canopies. The concepts of the p-theory have been reported and examined at the shoot and canopy scales, but not yet for the crown level. Currently, the p-value is estimated indirectly, such as converted from the spherically averaged silhouette to total area ratio ($\overline{STAR}$) or canopy transmittance measurements. In this work, we first validate the theoretical considerations of the p concept at the crown level (e.g., its relationship with $\overline{STAR}$), and then provide the first method to directly estimate photon recollision probability using Terrestrial Laser Scanning (TLS) data. The proposed geometric method is data-driven and avoids explicit reconstructions of tree structures. The p-value estimated here is the average recollision probability over spatial locations. We showed that the average recollision probability can be interpreted as the local spherical openness on phytoelement (leaf or needle) surfaces, which enabled a simple visibility calculation by avoiding explicit ray tracing. The developed method was tested on synthetic crowns of needle-leaved tree species, for which the reference p-values were known. Results confirmed the validity of the p-$\overline{STAR}$ relationship at the crown level, and showed that p-values can be accurately estimated from TLS point clouds with a relative root measure square error of less than 10%. This study displays the distinct advantage of TLS in delineating detailed tree crown structures and highlights its potential in studies of forest reflectance modeling.

1. Introduction

Physically-based remote sensing quantitatively predicts the interactions between solar radiation and vegetation (Huang et al., 2007). Two decades since its introduction, the spectral invariants theory (p-theory) has been widely applied in modeling the interaction of shortwave radiation with vegetation canopies (Knyazikhin et al., 1998). The p-theory states that canopy absorption, transmittance, and reflectance are determined only by the optical properties of foliage and spectrally invariant structural parameters. One of these parameters, photon recollision probability p, is found to be closely related to the solution of the classical three-dimensional (3D) radiative transfer equation that models the interactions between solar radiation and vegetation canopies (Ross, 1981; Knyazikhin et al., 1998).

The p-theory is a simple but powerful tool to model the canopy absorption, transmittance, and reflectance at any wavelength using the structural parameter p and the phytoelement (leaf or needle) albedo (Smolander and Stenberg, 2005; Stenberg, 2007; Rautiainen et al., 2009). When woody elements are considered, the albedo can be adjusted as an average value of albedos of phytoelement and woody elements weighted by their areas (Stenberg et al., 2013). Its usefulness, when applied in forward model simulations, depends on how well the p-value is related to other measurable vegetation attributes such as leaf area index (LAI). Stenberg (2007) proposed a simple analytical formula to calculate canopy average photon recollision probability from the total canopy interceptance in diffuse radiation. Later, this expression was validated by Rautiainen et al. (2009), who found a tight relationship between canopy interceptance and the effective LAI using extensive empirical data measured with the LAI-2000 Plant Canopy Analyzer. This relationship has also been integrated into the simple semi-physical forest reflectance model (PARAS), which was successfully used to simulate the absorption and reflectance of conifer canopies (Rautiainen and Stenberg, 2005; Manninen and Stenberg, 2009; Heiskanen et al., 2011; Schraik et al., 2019). So far, the p-value has been reported and examined both theoretically and empirically at the shoot and canopy scale (e.g., Smolander and Stenberg, 2003; Stenberg,

* Corresponding author.
E-mail address: di.wang@aalto.fi (D. Wang).

https://doi.org/10.1016/j.rse.2020.111932
Received 4 February 2020; Received in revised form 11 May 2020; Accepted 30 May 2020

2007). However, crown-level analysis remains unexplored.

The explicit estimation of photon recollision probability relies on two entries: 3D geometric models and photon tracking, which are impossible to materialize in reality (Stenberg et al., 2016). Terrestrial Laser Scanning (TLS, also known as terrestrial LiDAR), on the other hand, is able to provide detailed structural information through point clouds. The unique advantage of TLS for providing millimeter-level details even inside tree crowns makes it widely used in vegetation studies (Disney, 2019). These applications include forest inventory (Liang et al., 2018), tree topological reconstruction (Raumonen et al., 2013), leaf angle distribution estimation (Vicari et al., 2019b), LAI retrieval (Zhao et al., 2015), gap fraction assessment (Danson et al., 2007), and radiative transfer modeling (RTM) (Calders et al., 2018). Especially for RTM, TLS enables explicit 3D reconstructions of tree branching structures (Lau et al., 2018), which significantly improves the calibration and validation of EO data (Calders et al., 2018). These applications imply a great potential of using TLS to quantify tree crown structures. However, such a potential has not yet been explored for estimating the photon recollision probability.

In this paper, we aim to (a) validate the theoretical considerations of the photon recollision probability at the crown level (i.e., the relationship between p and $\overline{STAR}$), and (b) present the first method that directly estimates the photon recollision probability from synthetic TLS point clouds. Our method using TLS data avoids explicit geometric reconstructions of tree structures. This is important, because individual leaves or needles are challenging to recover. Instead, we model the volumetric occupancies of canopies with sphere covering, which leads to a simple calculation of spherical openness at specific viewpoints. The proposed method in this study provides a whole new way to directly estimate the photon recollision probability. Using realistic tree models and TLS simulations, we quantitatively show that this method is able to produce accurate p estimates for highly clumped needle crowns.

2. Theoretical background

The photon recollision probability p is a wavelength independent (i.e., spectrally invariant) structural parameter. Its intuitive interpretation is the probability that a photon will interact with the canopy again after being scattered from a phytoelement (e.g., leaf or needle) (Smolander and Stenberg, 2005).

Previous studies have shown that at canopy scale, p is able to link the canopy albedo (s), i.e., the fraction of intercepted radiation that is not absorbed, with the leaf or needle albedo (ω) at the specific wavelength λ by:

$$s(\lambda) = i_0 \frac{\omega(\lambda) - p\omega(\lambda)}{1 - p\omega(\lambda)}, \tag{1}$$

where i_0 is the canopy interceptance defined as the fraction of intercepted photons that are entering the canopy from above (Smolander and Stenberg, 2005; Rautiainen and Stenberg, 2005). Therefore, the amount of radiation absorbed or scattered by a canopy is determined by the wavelength-dependent average leaf or needle albedo, canopy interceptance, and the wavelength-independent structural parameter p.

The recollision probability p links the scattering properties at two consecutive hierarchical levels of a structure (Stenberg et al., 2016). For example, many broadleaf crowns have two structural levels consisting of single leaves and the crown itself. A photon scattered from a flat leaf will not interact with the same leaf again. Therefore, the overall crown albedo at a specific wavelength can be predicted from the leaf albedo at the same wavelength with the crown-level p-value. However, in a conifer crown, the clumping of needles into shoot introduces an additional hierarchical level. Similarly, the recollision probability can be defined for shoots (p_{sh}), which can be interpreted as the probability of a photon scattered from a needle interacting with the same shoot again. More generally, the recollision probability of a structure thus can be decomposed into different hierarchical levels as:

$$p = p_1 + (1 - p_1)p_2 + \ldots + (1 - p_{n-1})p_n, \tag{2}$$

where n is the number of hierarchical levels and p_i the recollision probability of a photon that has survived from the level $i - 1$ (Stenberg et al., 2016). For a specific hierarchical level i, the lower level $i - 1$ is called an element.

The recollision probability of a coniferous shoot was found to be linearly related to the spherically averaged silhouette to total area ratio ($\overline{STAR}$) in Monte Carlo simulations (Smolander and Stenberg, 2003). $\overline{STAR}$ is defined as:

$$\overline{STAR} = \frac{1}{\mathrm{TNA}} \frac{1}{4\pi} \int_{4\pi} \mathrm{SA}(\Omega)\mathrm{d}\Omega, \tag{3}$$

where TNA is the total needle area, SA(Ω) denotes the shoot silhouette area in direction Ω, and 4π represent all directions of the sphere. $STAR$ (Ω) is thus the silhouette to total area ratio in direction Ω (Oker-Blom and Smolander, 1988). The $\overline{STAR}$ of a convex body would be 1/4 (Lang, 1991). The ratio between spherically projected shoot area to spherically projected needle area is thus $4\overline{STAR}$ (Smolander and Stenberg, 2003) and is defined as the shoot shading factor (Stenberg, 1996). By assuming Lambertian reflectance, $4\overline{STAR}$ can be interpreted as the probability that a photon will escape the shoot after first interaction (Smolander and Stenberg, 2003; Rautiainen and Stenberg, 2005). Therefore, we have

$$p_{sh} = 1 - 4\overline{STAR}. \tag{4}$$

The equality of p_{sh} and $1 - 4\overline{STAR}$ is realized if the points of interaction are uniformly distributed over the needle surfaces of the shoot (i.e., spatial averaging) (Smolander and Stenberg, 2003).

The theory of photon recollision probability at shoot level was empirically tested by Rautiainen et al. (2012). They measured shoot and needle albedo, and shoot $\overline{STAR}$ (in order to calculate p-values) for Scots pine. The scaling effect of p-theory was thus examined. Results confirmed that a single structural parameter $\overline{STAR}$ (i.e., linearly related to p-value) could be used to scale the spectral albedos between a needle and a shoot. However, what remains unclear is the validity and effectiveness of the same method for scaling between shoot and crown levels, especially for structurally complex and very dense crowns (Stenberg et al., 2016).

3. Materials

Direct measurement of photon recollision probability is impossible, as it requires the tracking of individual photons inside the tree crown (Stenberg et al., 2016). Instead, physically realistic 3D models have been used as inputs for ray tracing approaches to sample and simulate the photon paths in the canopy. In this study, we created a series of virtual trees with different characteristics and calculated reference p values using ray tracing. Then, TLS point clouds were simulated based on these virtual models.

3.1. 3D virtual trees

In this study, 28 virtual mesh models of Scots pine (*Pinus sylvestris L.*) were created using the SpeedTree software (Interactive Data Visualization, Inc. Lexington, SC, USA). Each needle was shaped by an elongated triangle (Fig. 1). The average needle width was 4.1 mm, and length was 12.2 cm (Table 1). Each shoot was assembled by a twig with needles distributed following a phyllotactic arrangement (e.g., Smolander and Stenberg, 2003). For the creation of individual trees, we simulated different crown structures in order to capture the natural variations in tree size, leaf area, and clumping levels. Tree height ranged from 1.05 to 28.15 m, with a mean value of 9.31 m. In average, each tree was constructed of 281,988 needles, corresponding to 218 m^2 total needle area. We intentionally created trees covering an extreme range of $\overline{STAR}$ values (Fig. 2). The most clumped crown had a $\overline{STAR}$ of

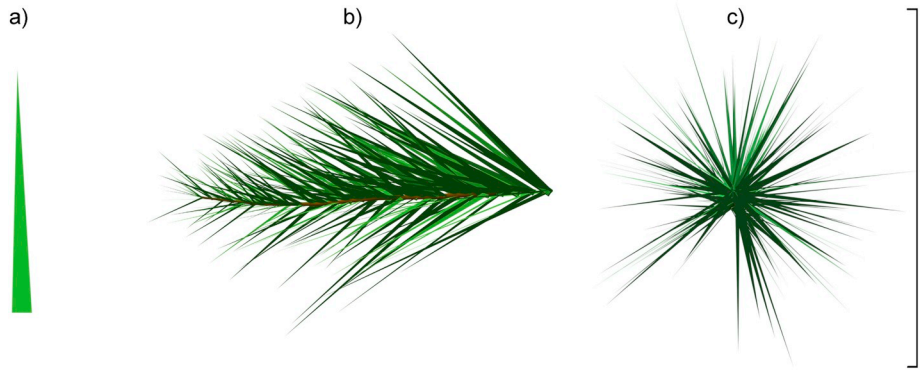

Fig. 1. Basic structures of a) a needle, b) a shoot (side view), and c) a shoot (top view). Shoot width is determined as the maximum dimension of top view.

0.02 (i.e., a *p*-value of 0.92), and the least clumped crown had a $\overline{STAR}$ of 0.19 (i.e., a *p*-value of 0.24). More details of individual trees can be found in Table 1. An example tree is shown in Fig. 3a. A visualization of all created trees can be found in Appendix A.

3.2. TLS simulation

TLS point clouds were simulated by using the open-source platform HELIOS (Bechtold and Höfle, 2016), a software that allows the simulation of various LiDAR sensors and platforms. We scanned each tree from four scan positions using the specifications of the Riegl VZ-400 (0.3 mrad beam divergence, 0.04° angular resolution, 10 m distance from the tree) (Fig. 4). The same grid positioning and angular resolution configurations were recommended for TLS data acquisition in forests and were deployed by previous simulation studies as well (Wilkes et al., 2017; Liu et al., 2019b). Point clouds obtained using 1, 2, and 4 scans were tested in this study (Fig. 4). An exemplary TLS point cloud with 4 scans is shown in Fig. 3c.

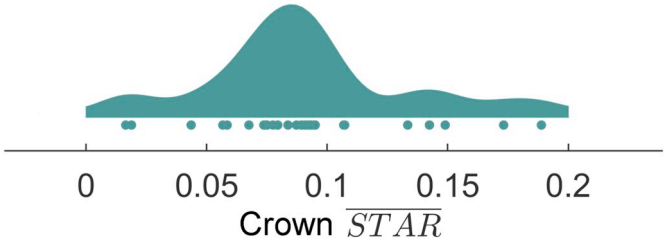

Fig. 2. Distribution of crown $\overline{STAR}$ values of the modeled trees.

4. Methods

4.1. $\overline{STAR}$ calculation

For mesh models, $\overline{STAR}$ can be explicitly determined by using Eq. 3. Specifically, the total needle area can be calculated by aggregating the two-sided surface area of each triangle mesh. To estimate the

Table 1
characteristics of the 28 Scots Pine trees.

TreeID	Height (m)	CD (m)	NW (cm)	NL (cm)	#Needle	TNA (m^2)	DBH (cm)	$\overline{STAR_s}$	$\overline{STAR_c}$
1	12.02	7.77	0.47	13.91	469,538	379.22	53.77	0.14	0.07
2	11.69	7.37	0.47	13.91	393,113	317.57	38.62	0.13	0.08
3	11.86	7.68	0.47	13.9	337,256	272.4	41.84	0.15	0.08
4	6.71	4.34	0.26	7.73	433,865	108.22	20.54	0.13	0.08
5	20.17	13.42	0.78	23.04	217,630	482.87	64.43	0.13	0.09
6	16.47	8.8	0.65	19.3	369,192	574.6	54.66	0.14	0.08
7	7.88	4.91	0.31	9.28	178,042	64.02	24.2	0.14	0.1
8	9.52	5.91	0.39	11.57	346,800	194.2	29.37	0.14	0.07
9	10.33	6.64	0.39	11.59	759,646	426.46	32.54	0.15	0.06
10	4.36	2.44	0.18	5.4	166,352	20.27	14.74	0.13	0.09
11	10.35	12.31	0.47	13.93	1,042,992	844.13	33.91	0.14	0.06
12	15.04	9.03	0.78	23.1	58,460	130.56	86.16	0.13	0.11
13	9.32	5.36	0.39	11.59	45,051	25.27	30	0.17	0.13
14	5	2.75	0.26	7.83	515,615	130.94	21.11	0.03	0.02
15	6.28	3.83	0.47	13.93	54,448	44.06	12.62	0.1	0.07
16	4.94	3.05	0.45	13.3	11,845	9.04	10.8	0.18	0.15
17	23.51	16.33	0.53	15.59	660,398	666.4	46.43	0.11	0.09
18	12.03	7.75	0.47	13.99	922,612	750.99	38.06	0.1	0.04
19	2.69	1.45	0.35	10.49	820	0.42	8.17	0.19	0.19
20	2.3	1.85	0.46	13.55	12,591	9.78	6.61	0.15	0.09
21	10.37	5.55	0.46	13.55	215,293	168.22	36.29	0.19	0.09
22	28.15	16.33	0.47	14.01	521,243	424.89	105.75	0.14	0.11
23	4.67	2.99	0.43	12.89	5067	3.74	12.14	0.2	0.17
24	7.49	4.07	0.47	13.86	49,427	39.8	29.64	0.14	0.09
25	2.41	1.56	0.23	6.97	27,399	5.56	6.57	0.14	0.09
26	2.23	1.61	0.23	6.95	54,301	10.96	5.72	0.14	0.07
27	1.79	1.26	0.14	4.17	17,265	1.25	3.69	0.16	0.12
28	1.05	0.59	0.05	1.38	9405	0.07	2.13	0.2	0.18
Mean	9.31	5.96	0.41	12.17	281,988	218.07	31.09	0.14	0.1

CD: crown diameter. NW: mean needle width. NL: mean needle length. TNA: total needle area. DBH: diameter at breast height. $\overline{STAR_s}$: shoot $\overline{STAR}$ (one randomly picked shoot from the crown). $\overline{STAR_c}$: crown $\overline{STAR}$.

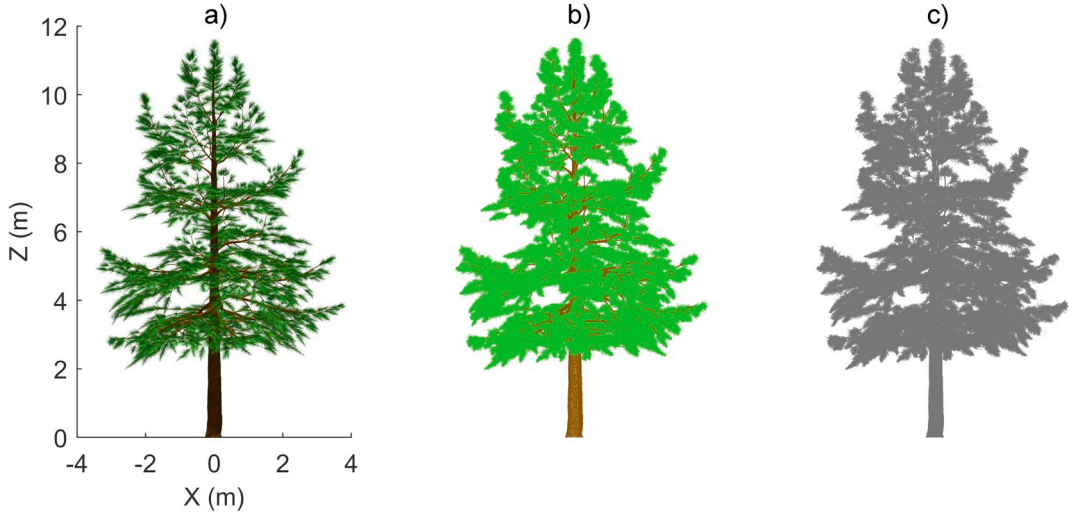

Fig. 3. a) A virtual Scots pine tree. b) Point cloud sampled from the mesh model (i.e., for visual comparison with the simulated TLS data). Green: needle. Brown: wood. c) Simulated TLS point cloud. (For interpretation of the references to colour in this figure legend, the reader is referred to the web version of this article.)

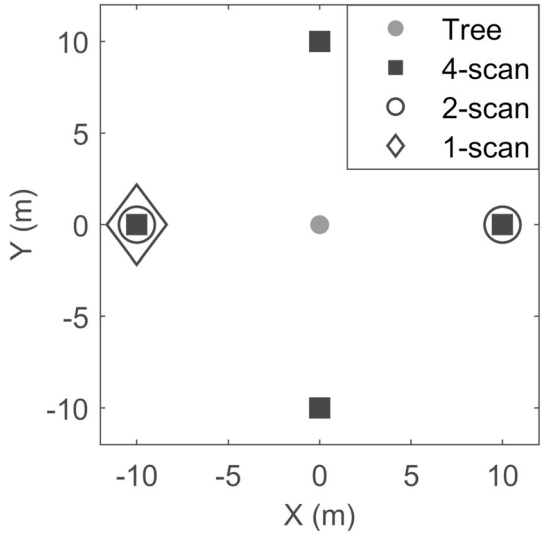

Fig. 4. Simulated TLS scan configurations.

directional distribution of the silhouette area, the mesh model is projected in 100 directions uniformly distributed over the hemisphere (Fig. 5a). For each direction, the explicit silhouette area can be estimated as the area of the union of projected triangles (Fig. 5b). Consequently, *STAR* of each projection direction is calculated. Integrating over all directions, $\overline{STAR}$ can be determined.

To further evaluate the influences of woody materials, we calculated $\overline{STAR}$ with and without those triangle meshes representing woody materials (i.e., twigs, branches and trunks), respectively. The same strategy was applied to each tree crown and a corresponding shoot sample that was randomly picked and manually extracted from the crown mesh models.

4.2. Average photon recollision probability

In this study, we view the concept of average photon recollision probability by assuming that anisotropic photons have reached phytoelement (leaf or needle) surfaces and are uniformly distributed (i.e., spatial averaging). This can be pictured as combining all scattering orders into a single scattering event. This interpretation is consistent with the assumption made in Smolander and Stenberg (2003), who derived the relationship between shoot level *p*-value and $\overline{STAR}$, and

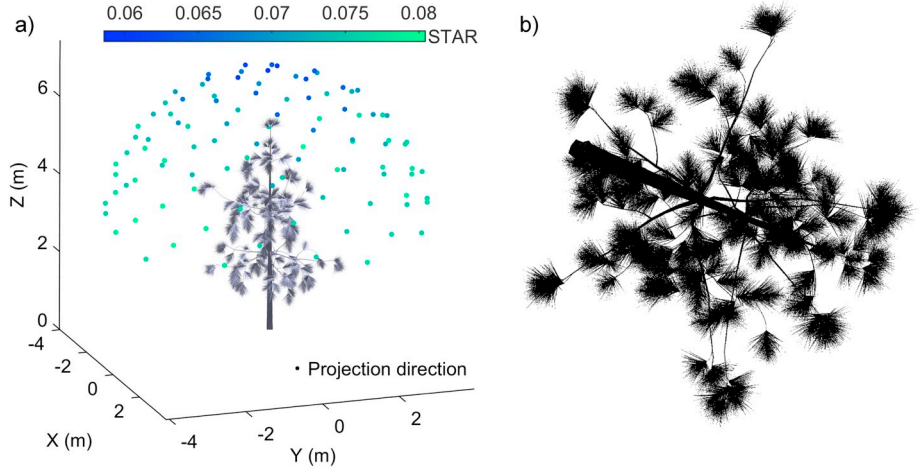

Fig. 5. Determination of $\overline{STAR}$. a) Directional distribution of *STAR*. b) Silhouette of the projected crown.

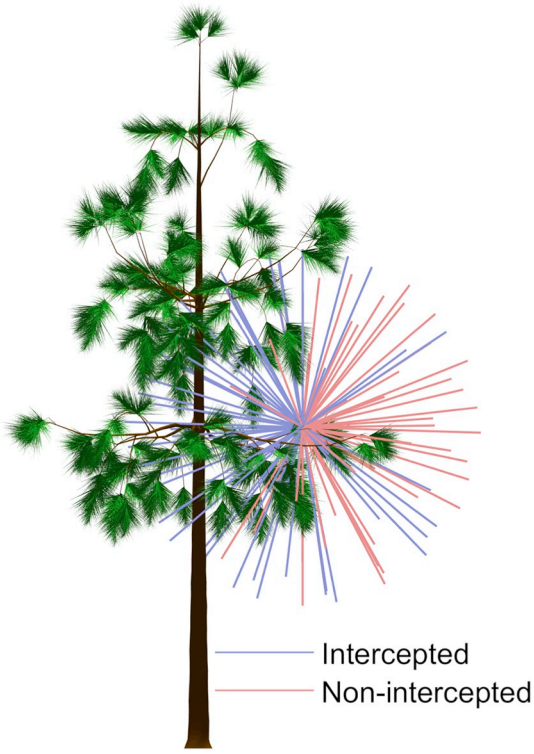

Fig. 6. Estimation of the average photon recollision probability using spherical openness.

also with Stenberg (2007), who proposed an analytical formula to calculate an average p-value from transmittance measures by averaging the recollision probability over points on all leaves. With anisotropic reflections, this interpretation is further equivalent to the spherical openness at the surface of a needle. Finally, we can similarly define the average photon recollision probability for a structure as the probability that anisotropic photons reflected from the surfaces of its elements interacting with current structure.

To calculate the average p, scattering positions should be first determined. In this study, three points are sampled for a needle surface. Specifically, each needle triangle is divided into three sub-triangles of equal area by connecting the vertices to the centroid. Then, the centroids of these three sub-triangles are regarded as the scattering points for the given needle. The area that a single scattering point occupies is also recorded (i.e., 1/3 of the needle surface area). For a single scattering point, the spherical openness is tested using virtual rays emitted into 100 directions uniformly distributed in the sphere (Fig. 6). The number of intercepted rays implies the localized p-value for current scattering point. The crown-level p-value is thus the average p over n scattering points, weighted by the occupied area a_i of each scattering point i as:

$$p_{crown} = \frac{\sum_{i=1}^{n} a_i p_i}{\sum_{i=1}^{n} a_i}. \quad (5)$$

4.3. Recollision probability from TLS point clouds

4.3.1. Sphere covering

A point cloud is inherently a collection of unordered 3D points and does not contain any topological and shape information, whereas conceptually the estimation of recollision probability requires the determination of whether a photon is intercepted or not. This requirement implies that volumetric shape information should be recovered first from point clouds. Overall, two approaches are available to retrieve solid shapes from point clouds. The first one is explicit 3D reconstruction, in which geometric primitives or mesh models are fitted into original points (e.g., Jenke et al., 2006). However, explicit reconstruction of tree crowns is impossible in practice. Tree crowns have very complex structures and irregular shapes. Moreover, point cloud density and quality are low inside crowns, due to severe occlusions when acquiring point clouds. It is commonly known that single leaves, especially needles, often cannot be resolved properly in the point clouds (Pfeifer et al., 2004). The second technique is voxelization that consolidates point clouds into 3D volumetric objects (e.g., Lecigne et al., 2017). Such voxel-based methods are useful in describing tree architectures. However, voxels produce excessively occlusive spaces, which is inapplicable for studying photon interceptance. For example, two connected voxels obstruct the entire space between points inside these two voxels. The recollision probability thus would be erroneously higher.

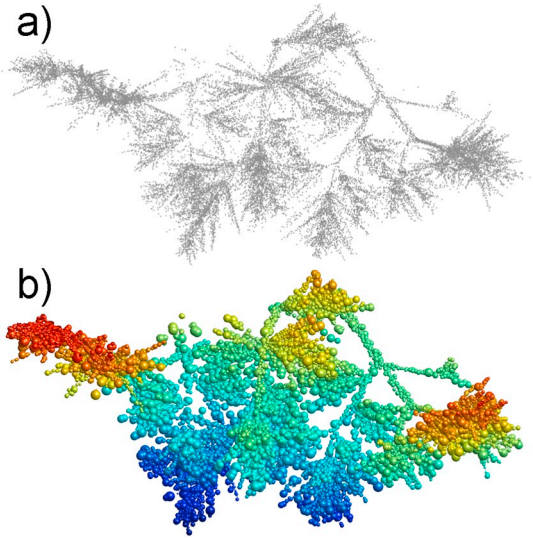

Fig. 7. Point cloud sphere covering. a) Original point cloud. b) Volumetric representation (colour denotes height, i.e., low = blue, high = red). (For interpretation of the references to colour in this figure legend, the reader is referred to the web version of this article.)

In this study, we use a sphere as the unit geometric primitive to model the 3D occupancies of point clouds. Specifically, a sphere is placed between a point and its nearest neighboring point. The sphere center is thus the mid-point and its radius is half the distance between two neighboring points. Spheres with very large radii are removed (i.e., larger than 99th percentile). This simple method to generate a volumetric representation from point clouds is called sphere covering (Fig. 7).

4.3.2. Recollision probability

We follow the same strategy as in Section 4.2 to estimate the average recollision probability for the volumetric sphere models. Scattering points are defined on needle surfaces as well. In this study, scattering points are directly extracted from corresponding mesh models. In practice, needle points should be identified first from point clouds so that the locations of scattering points can be determined. However, automatic leaf or needle identification is out of the focus of this study. It is noted that a number of methods are available to automatically extract leaf or needle points from point clouds (e.g., Ma et al., 2015; Wang et al., 2018, 2020; Vicari et al., 2019a). See Appendix C for an example.

For each scattering point, its local spherical openness can be calculated by testing the penetrability of virtual rays (Section 4.2). However, there are two challenges for directly applying such a strategy on the volumetric sphere model. First, individual needles are hardly resolved in the point clouds. The resulting volumetric model is thus not

detailed enough to estimate the p-value by regarding needles as the basic elements (e.g., Fig. 7). Second, the occlusion impact from the element itself should be eliminated. For example, a photon scattered from a leaf or needle surface will not interact with the same leaf or needle again. However, such object-level information is missing in point clouds and volumetric models.

We solve the first challenge on the level of details of point clouds by using the scaling property of p-theory (Eq. 2). In practice, shoots are usually well resolved in TLS point clouds. They can thus be regarded as the basic elements instead of needles. In particular, if we assume that p_{sh} is known, the crown-level average recollision probability p_{crown} can be estimated as:

$$p_{crown} = p_{sh} + (1 - p_{sh})p_{cw}, \tag{6}$$

where p_{cw} stands for the intermediate level p above shoots in a crown. This scaling approach uses shoots as elements and can be interpreted as the probability that a photon leaving a shoot will collide. The value of p_{sh} can be measured destructively or photographically using the procedure described in Stenberg et al. (2001) and Rautiainen et al. (2012). Moreover, we note that p_{sh} can also be estimated based on the same point cloud based method presented in this study, using data from high-precision techniques such as close-range LiDAR or tactile sensors. An example is given in Appendix B.

Second, to avoid self-occlusions, a simple strategy to exclude neighboring points is applied. For each scattering point, its neighboring points whose distances are closer than the shoot width are removed from collision analysis. The definition of shoot width is shown in Fig. 1. This simple strategy avoids the reconstruction of individual shoots.

4.3.3. TLS scan mode

The number of TLS scans affects the point cloud density and quality. Multiple scans provide denser point clouds and may avoid occlusions by acquiring data from different view positions. However, the density and spatial coverage of point clouds cannot be always guaranteed in practice, especially in extremely complex and clumped forests. To assess the impacts of TLS scans, we respectively tested the proposed method on TLS data from 1, 2, and 4 scan positions (Fig. 4). With 2 TLS scans, the scan positions were placed oppositely to ensure a good data coverage. Assuming that at least a fraction of the tree crown can be well captured by single-scan TLS, we hypothesized that the p-value can be estimated based on scattering points from those regions with dense point coverage. Therefore, for single-scan TLS data, only those scattering points distributed on the same side with (i.e., facing) the TLS scan location were estimated, as the opposite side was expected to have very sparse point coverage.

4.4. Assessment

The accuracy of estimated p-values are assessed using relative bias (Bias%) for individual trees, and the root mean square error (RMSE) and its relative value RMSE% for the entire dataset, calculated respectively as:

$$\text{Bias}_i\% = 100\% \times \frac{|p_i - \hat{p}_i|}{\hat{p}_i}, \tag{7}$$

$$\text{RMSE} = \sqrt{\frac{1}{n}\sum_{i=1}^{n}(p_i - \hat{p}_i)^2}, \tag{8}$$

$$\text{RMSE}\% = 100\% \times \frac{\text{RMSE}}{\bar{p}}, \tag{9}$$

where n is the number of observation data, $\hat{p}$ denotes the reference p-value and $\bar{p}$ is the mean value of reference p-values.

5. Results

5.1. Relationship between $\overline{STAR}$ and p

The relationship between $1 - 4\overline{STAR}$ and p was examined at the shoot and crown levels. By including woody materials in the $\overline{STAR}$ calculation, the discrepancies were large for both shoot and crown (Fig. 8a and c). On the other hand, a close to one to one relationship was found between the average recollision probability p and $1 - 4\overline{STAR}$ (Fig. 8b and d, when wood was excluded. These results confirmed the theoretical considerations of p and were consistent with previous studies on Scots pine shoots (Smolander and Stenberg, 2003). Our study showed that woody materials have a negative impact on the correspondence between p and $\overline{STAR}$. With the presence of woody materials, $1 - 4\overline{STAR}$ overestimated the p-value because the contribution of woody materials was more significant on the total area than silhouette area. Therefore, the estimated $\overline{STAR}$ was smaller than it should be. In addition, results showed that the relationship between $1 - 4\overline{STAR}$ and p was also valid for highly clumped needle crowns (Fig. 8d).

5.2. Quality of simulated TLS data

A quantitative accuracy analysis of the simulated TLS data showed that the average point cloud to mesh distance was 5 mm with a standard deviation of 6 mm. If we consider points with distances farther than three standard deviations (i.e., 3σ) from the mesh model as outliers (or ghost points), the point cloud had ~ 4% outliers (Fig. 9).

5.3. Crown-level p from TLS point clouds

We estimated crown-level p-values using the proposed sphere covering and scaling approach. Using data from four TLS scans yielded an RMSE of 0.059 (9.5%). The regression line had a slope of 0.99 (Fig. 10a). By reducing the scan positions to two, the RMSE stayed rather the same of 0.057 (9.1%). The slope was similarly at 0.98 (Fig. 10b). The result from single-scan TLS was marginally worse with an RMSE of 0.063 (10.1%). The slope of regression was reduced to 0.96 with a R^2 of 0.86 (Fig. 10c).

We additionally analyzed the impacts of number of scattering points by starting with 100 scattering points per crown and increasing the number to 1000 with an increment of 100. Results showed that the accuracy was improved with increased number of scattering points (Fig. 11). This was well expected, as more scattering points will better capture the overall structure of tree crowns. However, the improvement was minimal. The difference was smaller than 0.4% between using 100 and 1000 scattering points. Even with 5000 scattering points, the accuracy was only marginally improved. Therefore, 500 scattering points per tree was used in this study as a trade-off between accuracy and computational speed.

To further evaluate the impact of point density, we down-sampled each point cloud using voxels with the size from one to ten times the original average point spacing. The accuracy of p-value was evaluated for each down-sampled point cloud (Fig. 12). This analysis showed that clumped crowns (i.e., with high p-value) are robust against point density. In general, a minimum point spacing of 2 cm is recommended in practice.

5.4. Algorithm implementation and efficiency

We implemented our method in Matlab (The MathWorks, Inc.) and used parallel computing. In average, the processing time was 51 s for 1 million points on a laptop. The processing time had a linear relationship with the total number of points (Fig. 13). The laptop we used to run the algorithm has the following specifications: Windows 10, Intel® Core™ i7-8850H and 32 GB RAM.

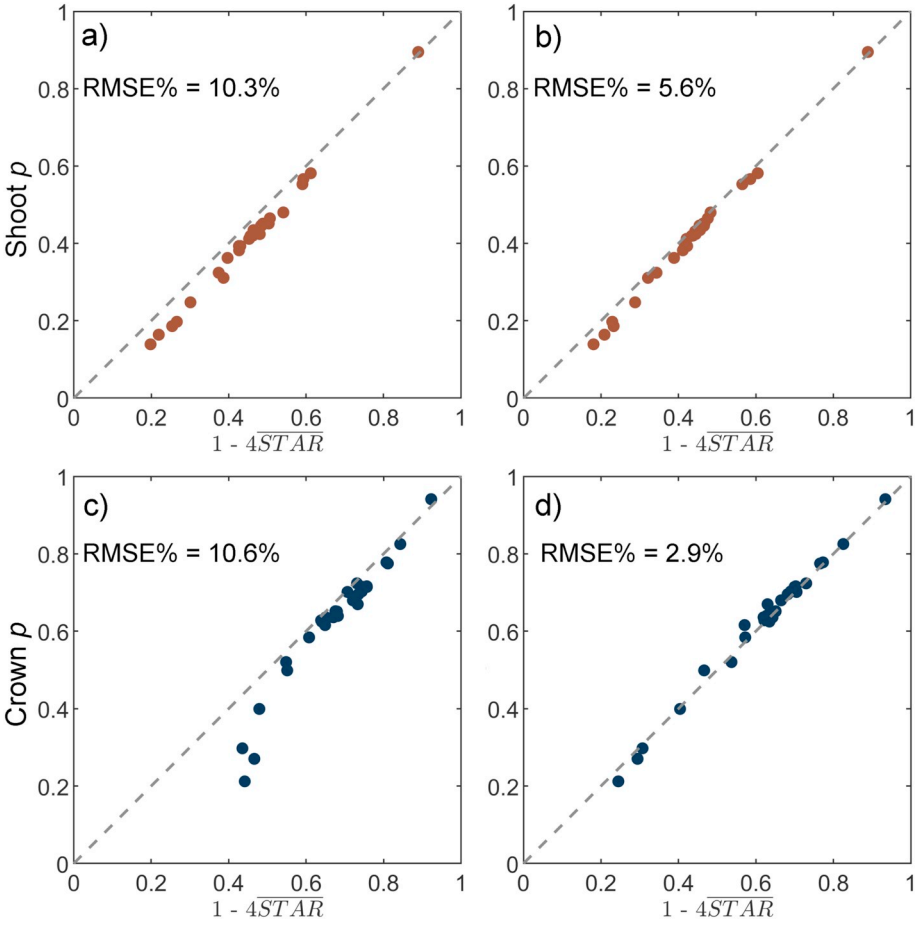

Fig. 8. Relation between $1 - 4\overline{STAR}$ and p for shoots a) with and b) without wood, and for crowns c) with and d) without wood.

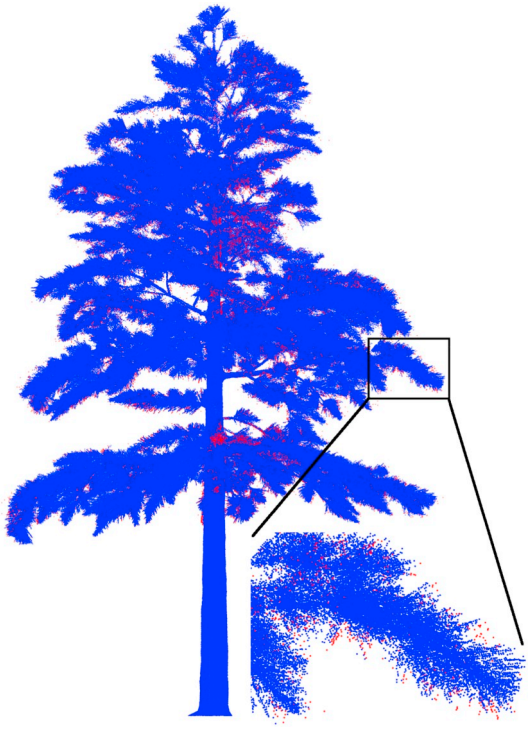

Fig. 9. Quality of the simulated TLS point cloud. Blue: inliers. Red: outliers (or ghost points). (For interpretation of the references to colour in this figure legend, the reader is referred to the web version of this article.)

6. Discussion

6.1. Photon recollision probability

Overall, the accuracy of spatially averaged recollision probability depends on how fast the recollision probability can converge to its limiting value, and how uniformly the points of interaction are distributed (Stenberg et al., 2016). The average p thus can be pictured as integrating all scattering orders as one event. In other words, photons are assumed to be uniformly distributed over the total needle area, and the scattering directions can be arbitrary. This interpretation leads to a simple calculation of local spherical openness, and is free from the impacts of directional distribution and interacting positions of scattered photons. The close to one to one relationship between p and $1 - 4\overline{STAR}$ for needle crowns also implied that the local spherical openness is indeed a good depiction of the average p (Fig. 8d). However, the limitation here is that it does not provide the recollision probability at each scattering orders, so that the corresponding contribution of each order is unknown. Moreover, since we did not rely on explicit 3D reconstructions of tree crowns, the directional distribution of photons cannot be tracked and determined. Nevertheless, directional p-values can be estimated by examining the interceptance of emitted photons in a certain direction in our method. This property might be linked to the new development of the spectral invariants theory on the directional area scattering factor (DASF) (Knyazikhin et al., 2013).

6.2. Estimation of p from TLS point clouds

Currently, the canopy-level p is estimated indirectly from LAI and the canopy transmittance in diffuse radiation (Stenberg, 2007). The

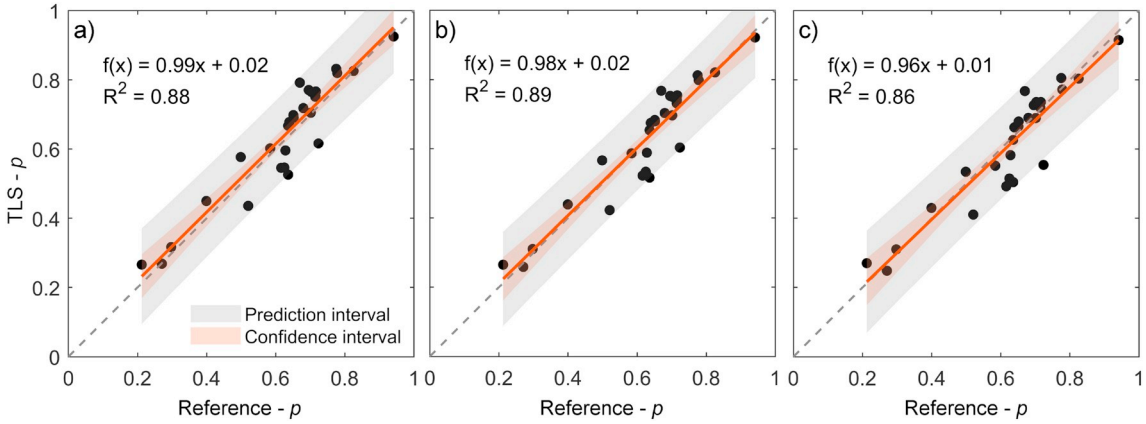

Fig. 10. Results of p estimation using TLS point clouds from a) 4 scans, b) 2 scans, and c) single-scan.

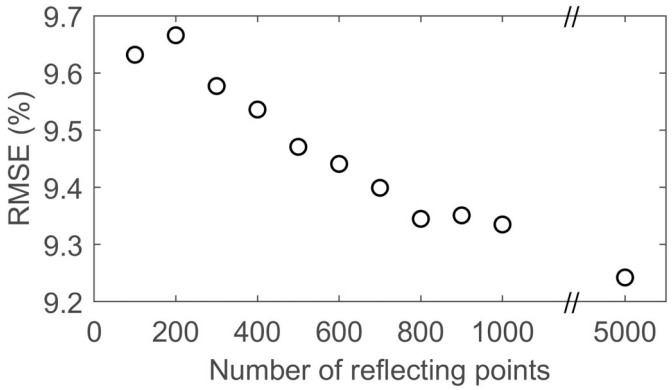

Fig. 11. Relative RMSE of p estimation with different number of scattering points.

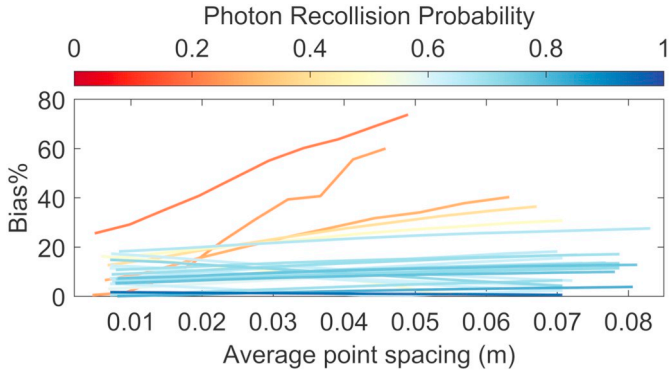

Fig. 12. The impact of point cloud density. Each curve represents an individual tree.

relationship between LAI and p can be quantitatively described using optical instruments (e.g., the LAI-2000 Plant Canopy Analyzer) (Rautiainen et al., 2009). To the best of our knowledge, no studies have reported direct p estimation methods. Thus, our study is the first attempt to directly estimate the photon recollision probability, which is made possible by the highly detailed structural information provided in TLS point clouds. Moreover, the p-values of individual tree crowns have not yet been properly examined before.

The designed sphere covering method is simple and intuitive. Intrinsically, it has the same mentality with point cloud voxelization, but uses spheres to model spatial occupancies. One of the advantages of using sphere packing is that the sizes of spheres are adaptive to point cloud density and distribution. This data-driven approach is more

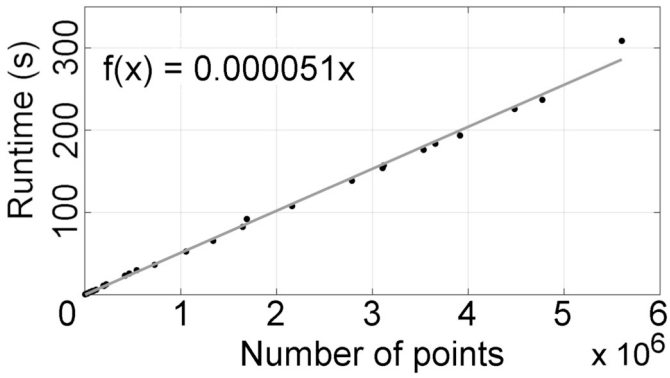

Fig. 13. The relationship between the runtime of our method with point cloud size.

robust than voxelization for which a voxel size should be defined. Previous studies have shown that voxel size has vital impacts on retrieving forest properties such as canopy gap fraction using TLS point clouds (Cifuentes et al., 2014). Moreover, the sphere covering method further eases the computation of interaction between virtual rays and volumetric objects. With spheres, the collision test corresponds to the calculation of the distance between a 3D point and a line, a step that could be easily parallelized. Therefore, our method requires light computational resources and short computation time (Fig. 13).

Although we used the scaling approach to estimate the crown-level p-value and treated shoots as basic elements (i.e., only above shoot level p was estimated with TLS), the proposed method is generic. Generally speaking, the recollision probability is only predictable by regarding the smallest resolvable structure in a point cloud as the basic element. In other words, TLS only estimates the p-value of structures at higher hierarchical levels than the smallest resolvable structure. Needleleaf crowns have at least three hierarchical structure levels of needle, shoot, and the crown itself. Since individual needles are almost impossible to be resolved in a point cloud in practice, the scaling approach has to be applied by treating shoots as basic elements. Indeed, if such a scaling approach is used, the shoot level recollision probability p_{sh} needs to be known in advance. For broadleaf crowns, this framework is straightforward as usually only two hierarchical structure levels exist (i.e, leaf and crown). The scaling approach is not necessary and the crown-level p can be directly calculated using leaves as basic elements, given that leaves are indeed resolved in the point clouds. Although we only tested our method on highly clumped needle crowns in this study using the scaling approach, the proposed generic framework is also applicable to leaf or needle level estimates without scaling, such as for broadleaf crowns or even needle crowns if needles are resolved in the point cloud. An example is given in Appendix B.

6.3. Model and TLS simulations

We relied on simulated tree models and TLS data in this study. The main reason was that the 'true' p-value is only known for synthetic models. Although in practice, p-values can be estimated from indirect methods such as measurements of LAI or converted from destructive measures of $\overline{STAR}$, their accuracies depend on the goodness of the p-theory itself and involve a certain level of uncertainty. Therefore, they cannot be used in this study to validate the concept of the estimated average recollision probability. However, future works should empirically look into the correspondences between p-values estimated from LAI measurements and our method using TLS data. It is also noted that in practice, the difficulties in detecting individual trees from TLS point clouds may introduce additional uncertainties in estimating the p-values at the single tree level. Despite the highly realistic tree models created in this study, our method in fact does not depend on the actual geometric characteristics of leaves/needles. We showed that the average recollision probability of uniformly distributed points in a tree crown is analogous to the local spherical openness, thus is independent from the actual shape or orientation of leaves/needles. Principally, this generic method only tests the spherical visibility from leaf or needle surfaces.

On the other hand, the HELIOS simulator used in this study resembles the real configurations of the Riegl VZ-400 scanner by considering the beam divergence, energy of the emitted pulse, atmospheric attenuation and the bidirectional reflectance distribution function (BRDF) surface reflectance model (Bechtold and Höfle, 2016). The resulting point clouds are expected to be very similar to real TLS point clouds and have been used in previous studies for estimating and validating leaf angle distributions (Liu et al., 2019a, 2019b). The quantitative accuracy analysis of the simulated TLS data (5 mm in Section 5.2) showed that the simulated accuracy lies within the manufacturer's specifications. Calders et al. (2017) showed that in practice, the range accuracy of the Riegl VZ-400 scanner is at the level of 1 to 2 mm at 10 m distance. Therefore, our simulation did not exaggerate the quality of TLS point clouds. This simulated quality is also consistent with real point clouds and previous analysis (Previtali et al., 2019). However, we note that the impacts from terrain accessibility, wind, atmospheric moisture, and occlusions are very difficult to simulate, which in practice, may cause additional challenges for the estimation of p-values. Nevertheless, the analyses on different TLS scan positions in this study partially mitigated this deficiency. We showed that even with single-scan TLS, the accuracy was still high with a relative RMSE of $\sim$ 10%. This implies that our method does not require a very high density point cloud. The recommended minimum point spacing of 2 cm in this study (Fig. 12) can be easily fulfilled by modern TLS instruments. Moreover, several trees in this study had very dense and clumped crowns, which led to occluded TLS point clouds inside crowns. The results were not affected, indicating that the proposed method is somewhat robust to occlusions as well, as long as the overall crown structure is captured by TLS.

6.4. Links to retrieval of biophysical variables from satellite data

Currently, clumping has not yet been rigorously included in many physically-based canopy reflectance (or radiative transfer) models that are used to retrieve biophysical variables from satellite data. Incorporating the effects of clumping in canopy reflectance models has posed a true challenge as very detailed canopy descriptions cannot readily be integrated into models operating at regional or global extents. Thus, especially for global applications, it is important to search for one or more key parameters that can capture the structure of a forest stand. Photon recollision probability has already been applied in the retrieval of biophysical properties from medium resolution Landsat 8 OLI and Sentinel-2 MSI data for entire forest stands (Schraik et al., 2019). Now, our new results show that it is possible to estimate directly p also for single trees from TLS data. This means, in turn, that the canopy reflectance modeling approach based on recollision probability has potential to be applied also in interpretation of higher spatial resolution remote sensing data.

7. Conclusion

The spectral invariants theory states that canopy scattering depends only on the optical properties of foliage and a spectrally invariant structural parameter - photon recollision probability p. This study presents a generic method that directly estimates the photon recollision probability from TLS point clouds. We interpret the concept of average photon recollision probability from a new perspective as the spherical openness on leaf or needle surfaces, which further enables a simple visibility test in TLS point clouds. The proposed method is free from restricted assumptions of tree architectures. We tested this method on synthetic models of needle-leaved trees and TLS data with 100% certain p-values. Results showed that the relationship between the photon recollision probability and $\overline{STAR}$ is valid for highly clumped needle crowns, and p-values can be accurately estimated from TLS point clouds with a relative RMSE of less than 10%. Future studies should aim to empirically evaluate the correspondences between p estimates from TLS and LAI measurements. With increasingly available TLS data for forests, this study strives to introduce a new approach to accurately estimate the photon recollision probability, and can facilitate the application of the spectral invariants theory in modeling the shortwave radiation regime of vegetation. Moreover, accounting for vegetation clumping through concepts such as $\overline{STAR}$ is fundamental in producing operationally e.g., more accurate global maps of vegetation from satellite data.

Declaration of Competing Interest

The authors declare that they have no known competing financial interests or personal relationships that could have appeared to influence the work reported in this paper.

Acknowledgments

Di Wang was supported by a postdoctoral fellowship of the School of Engineering, Aalto University. This study received funding from the European Research Council (ERC) under the European Union's Horizon 2020 research and innovation programme (grant agreement No 771049). The text reflects only the authors' view and the Agency is not responsible for any use that may be made of the information it contains.

Appendix A. Supplementary data

Supplementary data to this article can be found online at https://doi.org/10.1016/j.rse.2020.111932.

Appendix B. Shoot p estimation from point clouds

In this section, we report experiment results of p estimates for shoots. The purpose of this experiment was to evaluate the universality of the proposed method using point clouds without scaling.

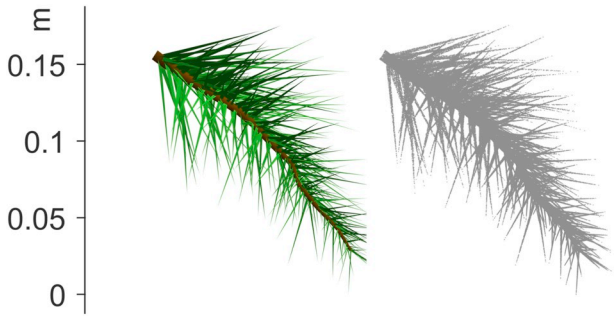

Fig. B.14. An exemplary Shoot model (left) and its corresponding sampled 'perfect' point cloud (right).

In this example, the basic element was a needle. In practice, individual needles are unlikely resolved in a TLS point cloud, due to the small size and data occlusions introduced by mutual shading. Therefore, we directly sampled point clouds from the mesh models. Specifically, for each triangle polygon (i.e., needle), a point was sampled per mm^2. The resulting point cloud was thus denoted as a 'perfect' point cloud (Fig. B.14). This sampling routine was to simulate those point clouds in which individual leaf or needle is resolved.

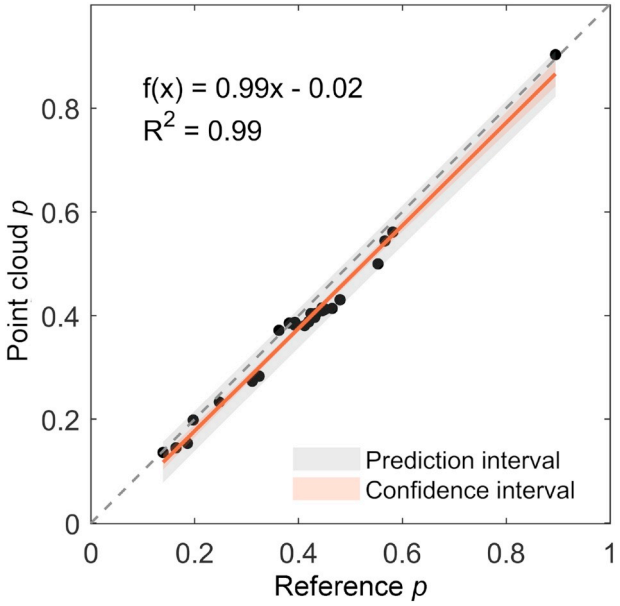

Fig. B.15. Results of shoot photon recollision probability estimation with needles as elements.

We then applied the proposed method on such 'perfect' point clouds, and treated needles as basic elements. The same sphere covering and spherical openness test were exercised. This test yielded a RMSE of 0.063 with a relative RMSE of 7.3%. The results in Fig. B.15 showed a high agreement between point clouds estimated and reference *p*-values, implying that our method is indeed generic.

In summary, our method treats the smallest resolvable structure in the point clouds as basic elements, and estimates the photon recollision probability of the structures at higher hierarchical levels than the smallest resolvable structure. If the smallest resolvable structure is beyond phytoelements (leaf or needle), the scaling approach (Eq. 2) has to be applied.

Appendix C. Automatic determination of scattering points

In this section, we report experiment results of crown *p* estimates based on scattering points that were automatically determined from TLS point clouds.

In this study, the scattering points are theoretically defined on phytoelement (leaf or needle) surfaces. Therefore, in order to determine the locations of scattering points, leaf or needle points should be detected first. We applied an unsupervised and automatic leaf-wood separation method to exclude wood points in TLS point clouds (Wang et al., 2020). This method successfully separated dominant woody structures from phytoelement (Fig. C.16).

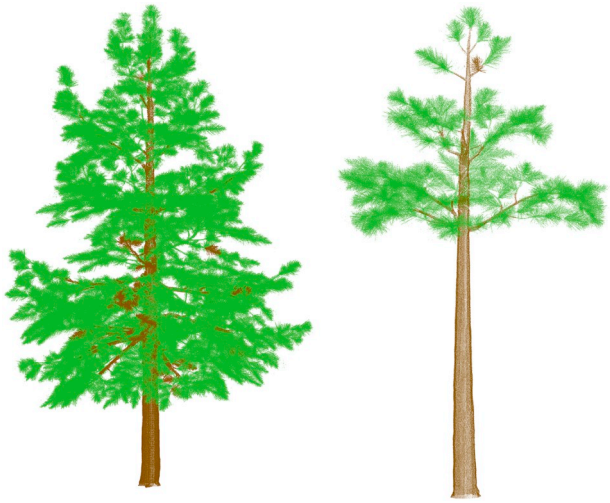

Fig. C.16. Examples of automatically separated woody structures (brown) and phytoelements (green) in TLS point clouds. (For interpretation of the references to colour in this figure legend, the reader is referred to the web version of this article.)

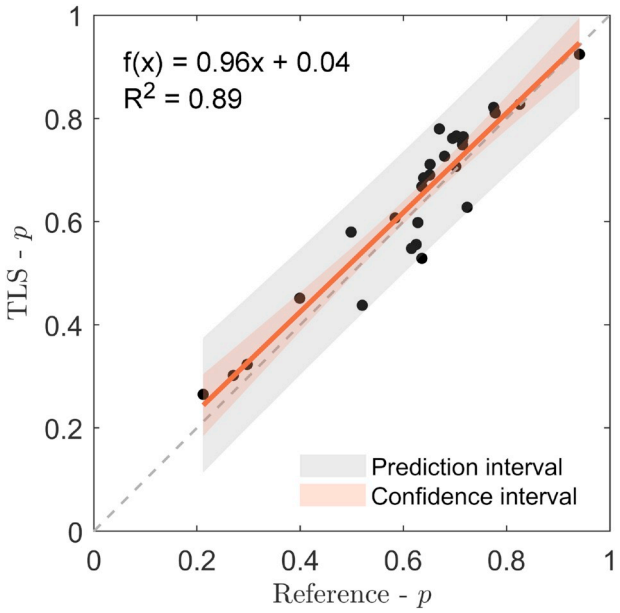

Fig. C.17. Results of crown photon recollision probability estimations with automatically defined scattering points.

To be consistent with the number of scattering points sampled from mesh models used in the main body of this paper, 500 random points per tree were selected from those detected phytoelement points as scattering points. Subsequently, the same spherical covering and scaling methods were applied to estimate the crown-level p values.

Results were first compared with reference values (Fig. C.17). This experiment yielded an RMSE of 0.057 with a relative RMSE of 9.2%. The results were very similar to those using scattering points directly from the mesh models (9.5%) (Fig. 10). We thus conclude that the exact locations of scattering points are not significant, and they can be determined fully automatically in point clouds, without the help of mesh models. Moreover, this observation was also partially justified by the results obtained from using only single-scan TLS data (Fig. 10).

References

Bechtold, S., Höfle, B., 2016. HELIOS: a multi-purpose lidar simulation framework for research, planning and training of laser scanning operations with airborne, ground-based mobile and stationary platforms. ISPRS Annals of Photogrammetry, Remote Sensing and Spatial Information Sciences III-3, 161–168. https://doi.org/10.5194/isprs-annals-III-3-161-2016.

Calders, K., Disney, M., Armston, J., Burt, A., Brede, B., Origo, N., Muir, J., Nightingale, J., 2017. Evaluation of the range accuracy and the radiometric calibration of multiple terrestrial laser scanning instruments for data interoperability. IEEE Trans. Geosci. Remote Sens. 55, 2716–2724.

Calders, K., Origo, N., Burt, A., Disney, M., Nightingale, J., Raumonen, P., Åkerblom, M., Malhi, Y., Lewis, P., 2018. Realistic forest stand reconstruction from terrestrial lidar for radiative transfer modelling. Remote Sens. 10, 933.

Cifuentes, R., Van der Zande, D., Farifteh, J., Salas, C., Coppin, P., 2014. Effects of voxel size and sampling setup on the estimation of forest canopy gap fraction from terrestrial laser scanning data. Agric. For. Meteorol. 194, 230–240.

Danson, F.M., Hetherington, D., Morsdorf, F., Koetz, B., Allgower, B., 2007. Forest canopy gap fraction from terrestrial laser scanning. IEEE Geosci. Remote Sens. Lett. 4, 157–160.

Disney, M., 2019. Terrestrial lidar: a three-dimensional revolution in how we look at trees. New Phytol. 222, 1736–1741.

Heiskanen, J., Rautiainen, M., Korhonen, L., Mõttus, M., Stenberg, P., 2011. Retrieval of boreal forest lai using a forest reflectance model and empirical regressions. Int. J. Appl. Earth Obs. Geoinf. 13, 595–606.

Huang, D., Knyazikhin, Y., Dickinson, R.E., Rautiainen, M., Stenberg, P., Disney, M., Lewis, P., Cescatti, A., Tian, Y., Verhoef, W., et al., 2007. Canopy spectral invariants for remote sensing and model applications. Remote Sens. Environ. 106, 106–122.

Jenke, P., Wand, M., Bokeloh, M., Schilling, A., Straßer, W., 2006. Bayesian point cloud reconstruction, in: computer graphics forum. Wiley Online Library 379–388.

Knyazikhin, Y., Martonchik, J., Myneni, R.B., Diner, D., Running, S.W., 1998. Synergistic

algorithm for estimating vegetation canopy leaf area index and fraction of absorbed photosynthetically active radiation from MODIS and MISR data. Journal of Geophysical Research: Atmospheres 103, 32257–32275.
Knyazikhin, Y., Schull, M.A., Stenberg, P., Mõttus, M., Rautiainen, M., Yang, Y., Marshak, A., Carmona, P.L., Kaufmann, R.K., Lewis, P., et al., 2013. Hyperspectral remote sensing of foliar nitrogen content. Proc. Natl. Acad. Sci. 110, E185–E192.
Lang, A., 1991. Application of some of cauchy's theorems to estimation of surface areas of leaves, needles and branches of plants, and light transmittance. Agric. For. Meteorol. 55, 191–212.
Lau, A., Bentley, L.P., Martius, C., Shenkin, A., Bartholomeus, H., Raumonen, P., Malhi, Y., Jackson, T., Herold, M., 2018. Quantifying branch architecture of tropical trees using terrestrial lidar and 3d modelling. Trees 32, 1219–1231.
Lecigne, B., Delagrange, S., Messier, C., 2017. Exploring trees in three dimensions: Voxr, a novel voxel-based r package dedicated to analysing the complex arrangement of tree crowns. Ann. Bot. 121, 589–601.
Liang, X., Hyyppä, J., Kaartinen, H., Lehtomäki, M., Pyörälä, J., Pfeifer, N., Holopainen, M., Brolly, G., Francesco, P., Hackenberg, J., et al., 2018. International benchmarking of terrestrial laser scanning approaches for forest inventories. ISPRS J. Photogramm. Remote Sens. 144, 137–179.
Liu, J., Skidmore, A.K., Wang, T., Zhu, X., Premier, J., Heurich, M., Beudert, B., Jones, S., 2019a. a. Variation of leaf angle distribution quantified by terrestrial lidar in natural european beech forest. ISPRS J. Photogramm. Remote Sens. 148, 208–220.
Liu, J., Wang, T., Skidmore, A.K., Jones, S., Heurich, M., Beudert, B., Premier, J., 2019b. b. Comparison of terrestrial lidar and digital hemispherical photography for estimating leaf angle distribution in european broadleaf beech forests. ISPRS J. Photogramm. Remote Sens. 158, 76–89.
Ma, L., Zheng, G., Eitel, J.U., Moskal, L.M., He, W., Huang, H., 2015. Improved salient feature-based approach for automatically separating photosynthetic and non-photosynthetic components within terrestrial lidar point cloud data of forest canopies. IEEE Trans. Geosci. Remote Sens. 54, 679–696.
Manninen, T., Stenberg, P., 2009. Simulation of the effect of snow covered forest floor on the total forest albedo. Agric. For. Meteorol. 149, 303–319.
Oker-Blom, P., Smolander, H., 1988. The ratio of shoot silhouette area to total needle area in scots pine. For. Sci. 34, 894–906.
Pfeifer, N., Gorte, B., Winterhalder, D., et al., 2004. Automatic reconstruction of single trees from terrestrial laser scanner data. In: Proceedings of 20th ISPRS congress, ISPRS Istanbul, pp. 114–119.
Previtali, M., Daz-Vilariño, L., Scaioni, M., Fras, E., et al., 2019. Evaluation of the expected data quality in laser scanning surveying of archaeological sites. In: 2019 IMEKO TC-4 Int. Conf. On metrology for archeology and cultural heritage (METROARCHEO2019), pp. 19–24.
Raumonen, P., Kaasalainen, M., Åkerblom, M., Kaasalainen, S., Kaartinen, H., Vastaranta, M., Holopainen, M., Disney, M., Lewis, P., 2013. Fast automatic precision tree models from terrestrial laser scanner data. Remote Sens. 5, 491–520.
Rautiainen, M., Stenberg, P., 2005. Application of photon recollision probability in coniferous canopy reflectance simulations. Remote Sens. Environ. 96, 98–107.
Rautiainen, M., Mõttus, M., Stenberg, P., 2009. On the relationship of canopy lai and photon recollision probability in boreal forests. Remote Sens. Environ. 113, 458–461.
Rautiainen, M., Mõttus, M., Yáñez-Rausell, L., Homolová, L., Malenovsk, Z., Schaepman, M.E., 2012. A note on upscaling coniferous needle spectra to shoot spectral albedo. Remote Sens. Environ. 117, 469–474.
Ross, J., 1981. The Radiation Regime and Architecture of Plant Stands. Dr W. Junk Publishers, The Hague, Netherlands.
Schraik, D., Varvia, P., Korhonen, L., Rautiainen, M., 2019. Bayesian inversion of a forest reflectance model using sentinel-2 and landsat 8 satellite images. J. Quant. Spectrosc. Radiat. Transf. 233, 1–12.
Smolander, S., Stenberg, P., 2003. A method to account for shoot scale clumping in coniferous canopy reflectance models. Remote Sens. Environ. 88, 363–373.
Smolander, S., Stenberg, P., 2005. Simple parameterizations of the radiation budget of uniform broadleaved and coniferous canopies. Remote Sens. Environ. 94, 355–363.
Stenberg, P., 1996. Correcting lai-2000 estimates for the clumping of needles in shoots of conifers. Agric. For. Meteorol. 79, 1–8.
Stenberg, P., 2007. Simple analytical formula for calculating average photon recollision probability in vegetation canopies. Remote Sens. Environ. 109, 221–224.
Stenberg, P., Palmroth, S., Bond, B.J., Sprugel, D.G., Smolander, H., 2001. Shoot structure and photosynthetic efficiency along the light gradient in a scots pine canopy. Tree Physiol. 21, 805–814.
Stenberg, P., Lukeš, P., Rautiainen, M., Manninen, T., 2013. A new approach for simulating forest albedo based on spectral invariants. Remote Sens. Environ. 137, 12–16.
Stenberg, P., Mõttus, M., Rautiainen, M., 2016. Photon recollision probability in modelling the radiation regime of canopies—a review. Remote Sens. Environ. 183, 98–108.
Vicari, M.B., Disney, M., Wilkes, P., Burt, A., Calders, K., Woodgate, W., 2019a. Leaf and wood classification framework for terrestrial lidar point clouds. Methods Ecol. Evol. 10, 680–694.
Vicari, M.B., Pisek, J., Disney, M., 2019b. New estimates of leaf angle distribution from terrestrial lidar: comparison with measured and modelled estimates from nine broadleaf tree species. Agric. For. Meteorol. 264, 322–333.
Wang, D., Brunner, J., Ma, Z., Lu, H., Hollaus, M., Pang, Y., Pfeifer, N., 2018. Separating tree photosynthetic and non-photosynthetic components from point cloud data using dynamic segment merging. Forests 9, 252.
Wang, D., Momo Takoudjou, S., Casella, E., 2020. Lewos: a universal leaf-wood classification method to facilitate the 3d modelling of large tropical trees using terrestrial lidar. Methods Ecol. Evol. 11, 376–389. https://doi.org/10.1111/2041-210X.13342.
Wilkes, P., Lau, A., Disney, M., Calders, K., Burt, A., de Tanago, J.G., Bartholomeus, H., Brede, B., Herold, M., 2017. Data acquisition considerations for terrestrial laser scanning of forest plots. Remote Sens. Environ. 196, 140–153.
Zhao, K., Garca, M., Liu, S., Guo, Q., Chen, G., Zhang, X., Zhou, Y., Meng, X., 2015. Terrestrial lidar remote sensing of forests: maximum likelihood estimates of canopy profile, leaf area index, and leaf angle distribution. Agric. For. Meteorol. 209, 100–113.